Supplemental Materials for "A one-step fabrication of soft-magnetic high entropy alloy fiber with excellent strength and flexibility"

Yan Ma[1, 2, †], Zongde Kou[3, †], Weiming Yang[1,*], Aina He[2], Yaqiang Dong[2], Qikui Man[2], Haishun Liu[4], Zhiming Li[5], Akihisa Inoue[6], and Jiawei Li[2,*]

[1]School of Mechanics and Civil Engineering, State Key Laboratory for Geomechanics and Deep Underground Engineering, China University of Mining and Technology, Xuzhou 221116, China

[2]CAS Key Laboratory of Magnetic Materials and Devices, Zhejiang Province Key Laboratory of Magnetic Materials and Application Technology, Ningbo Institute of Materials Technology and Engineering, Chinese Academy of Sciences, Ningbo, Zhejiang 315201, China

[3]Herbert Gleiter Institute of Nanoscience, School of Material Science and Engineering, Nanjing University of Science and Technology, Nanjing 210094, China

[4]School of Materials and Physics, China University of Mining and Technology, Xuzhou 221116, China

[5]School of Materials Science and Engineering, Central South University, Changsha, 410083, China

[6]International Institute of Green Materials, Josai International University, Togane, 283-8555, Japan

This file includes:

† These authors made equal contributions: Y. Ma, Z.D. Kou.

* To whom correspondence should be addressed. wmyang@cumt.edu.cn (W.M. Yang), and lijw@nimte.ac.cn (J.W. Li)

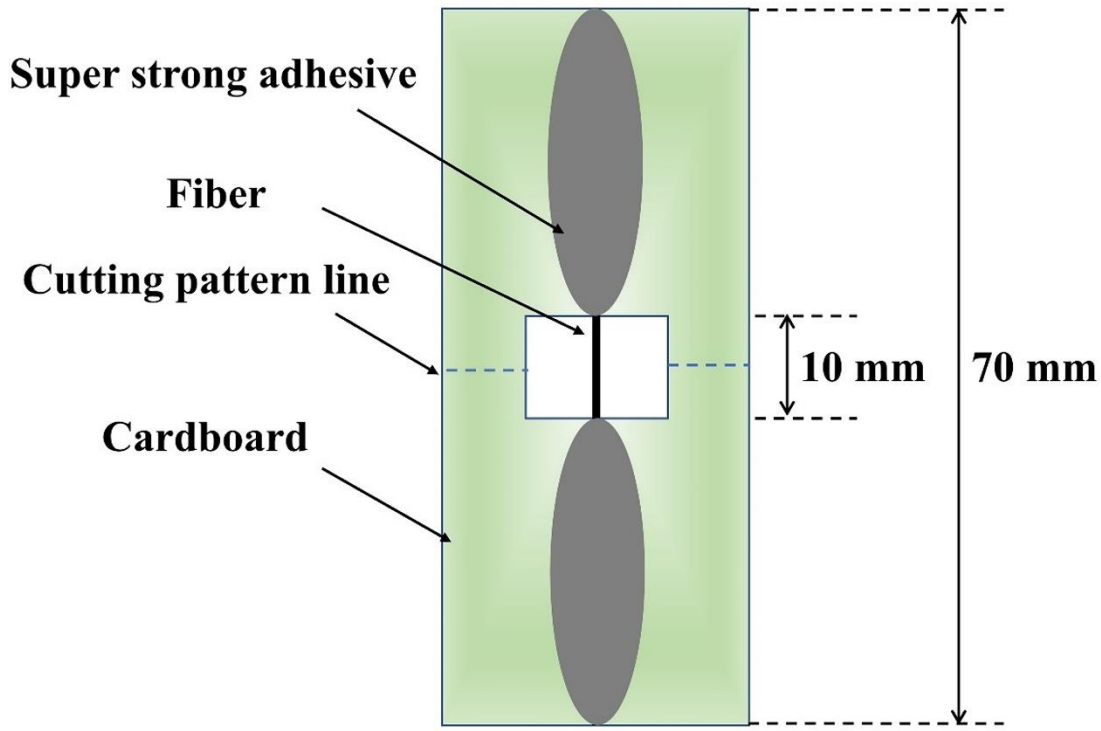

Figure S1. Tensile test samples of HEA fibers according to the ASTM D3379-75 standard.

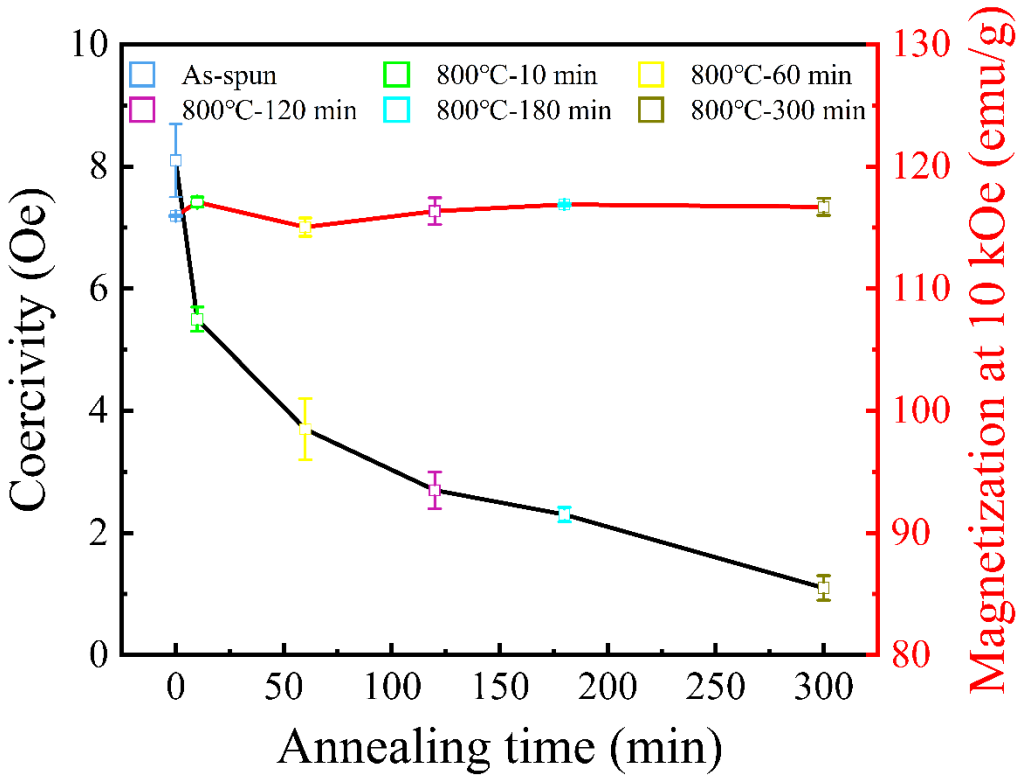

Figure S2. Annealing time dependence of M_s and H_c of HEA fibers. Error bars refer to the standard deviations of three experiment. Source data for Figure S2 are provided as a Source data file.

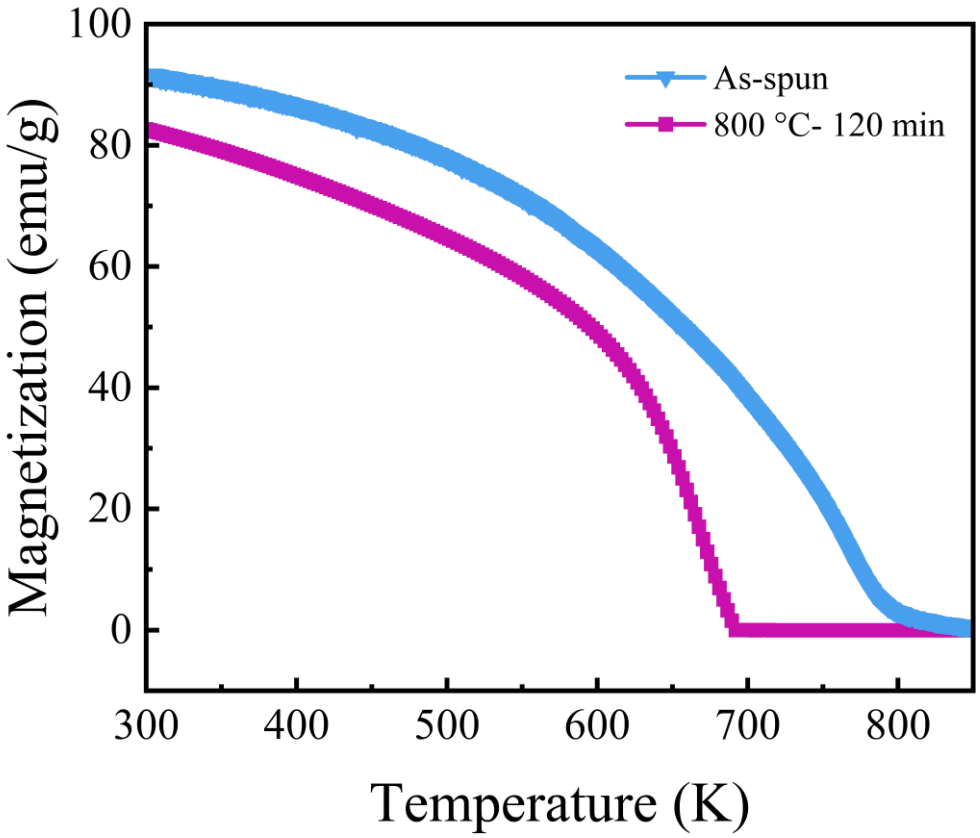

Figure S3. *M-T* curves measured in the temperature range 300–850 K under a magnetic field of 1000 Oe of as-spun and 800 ℃-120 min annealed HEA fibers. Source data for Figure S3 are provided as a Source data file.

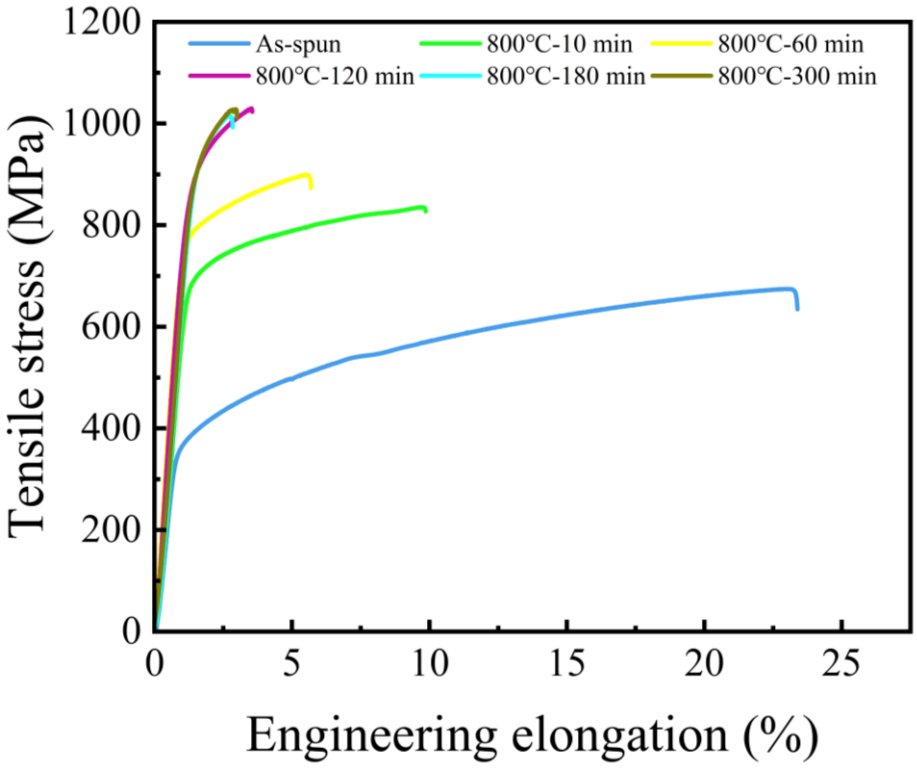

Figure S4. Tensile stress-strain curves of HEA fibers with different annealing time. Source data for Figure S4 are provided as a Source data file.

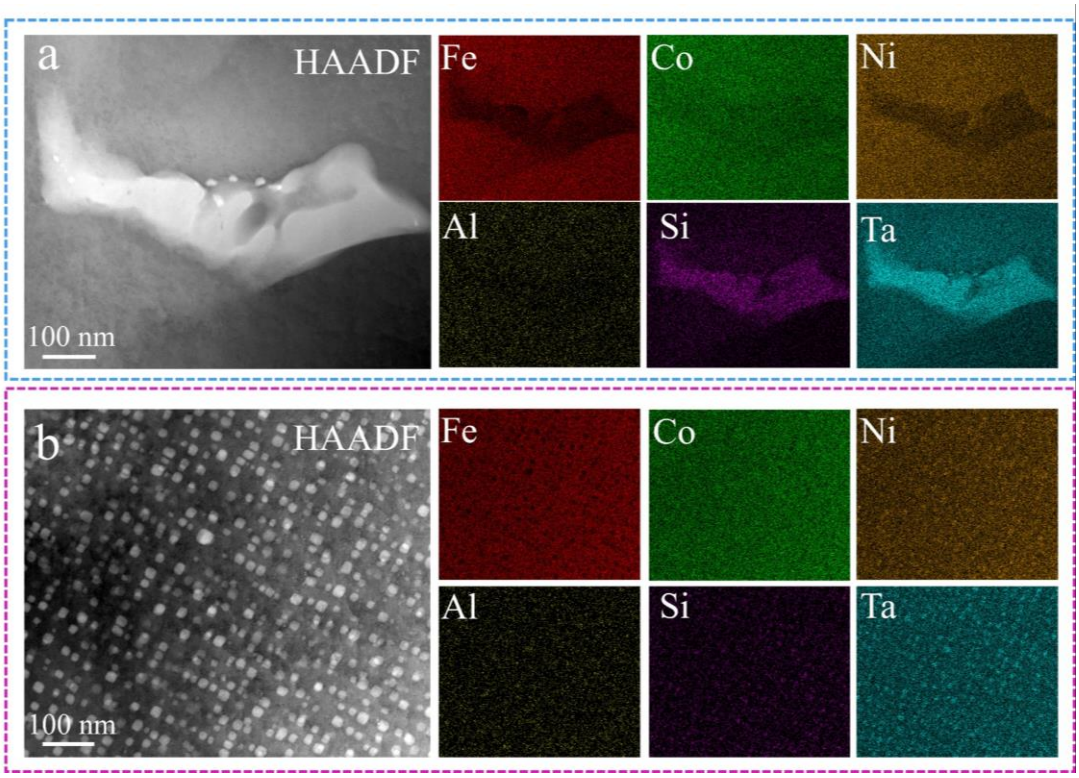

Figure S5. HAADF-STEM images of **a** as-spun and **b** 800 ℃-120 min annealed HEA fibers with accompanying high-resolution EDX images.

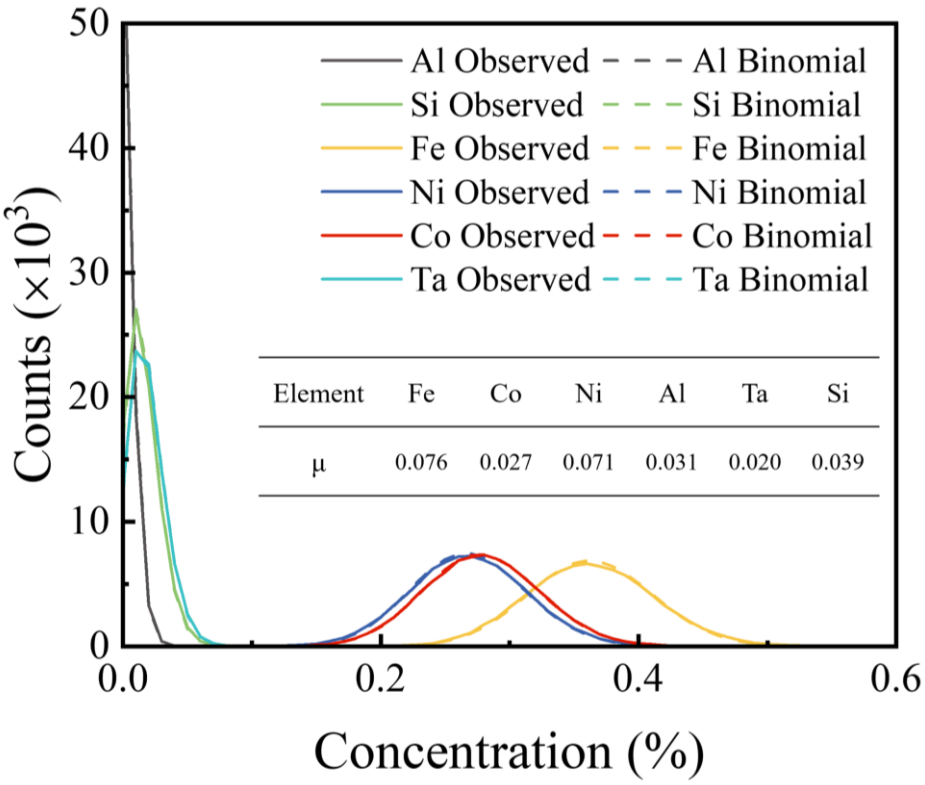

Figure S6. Frequency distribution analysis confirming the random distribution of the elements of as-spun HEA fibers from APT analysis. Source data for Figure S6 are provided as a Source data file.

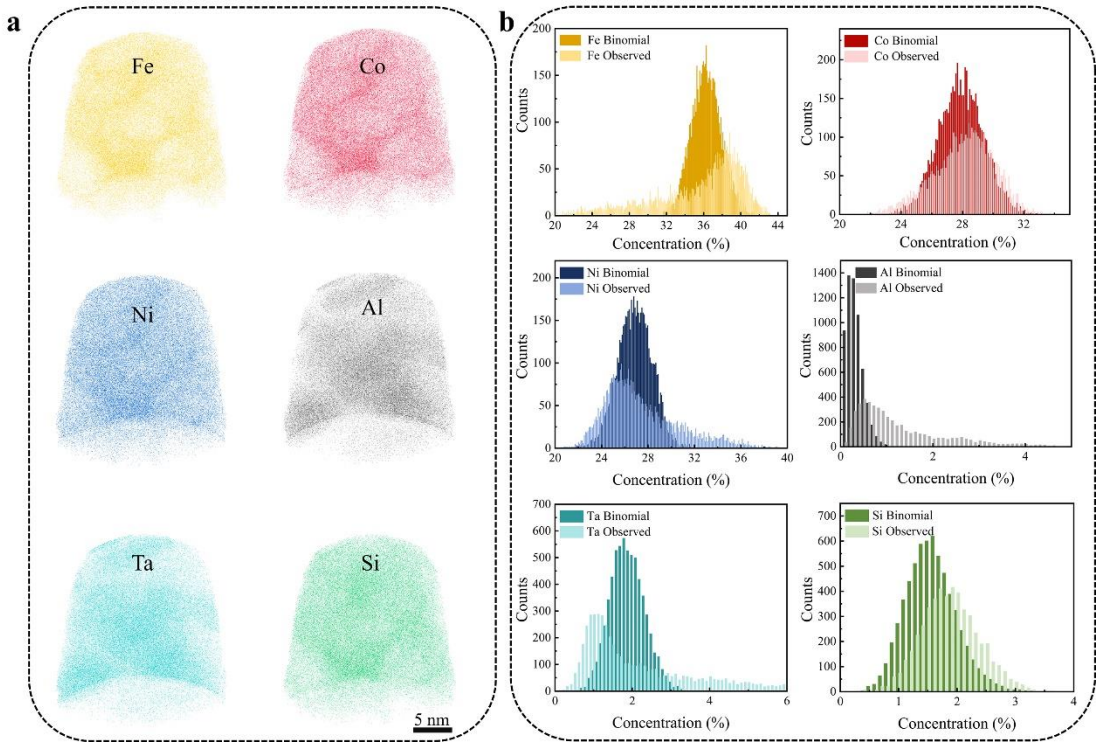

Figure S7. APT analysis of 800 ℃-120 min annealed HEA fibers. a 3D reconstruction maps of a typical APT tip showing the uniform distribution of all elements in near atomic-scale. **b** Frequency distribution curves and the fitted binomial distribution curves.

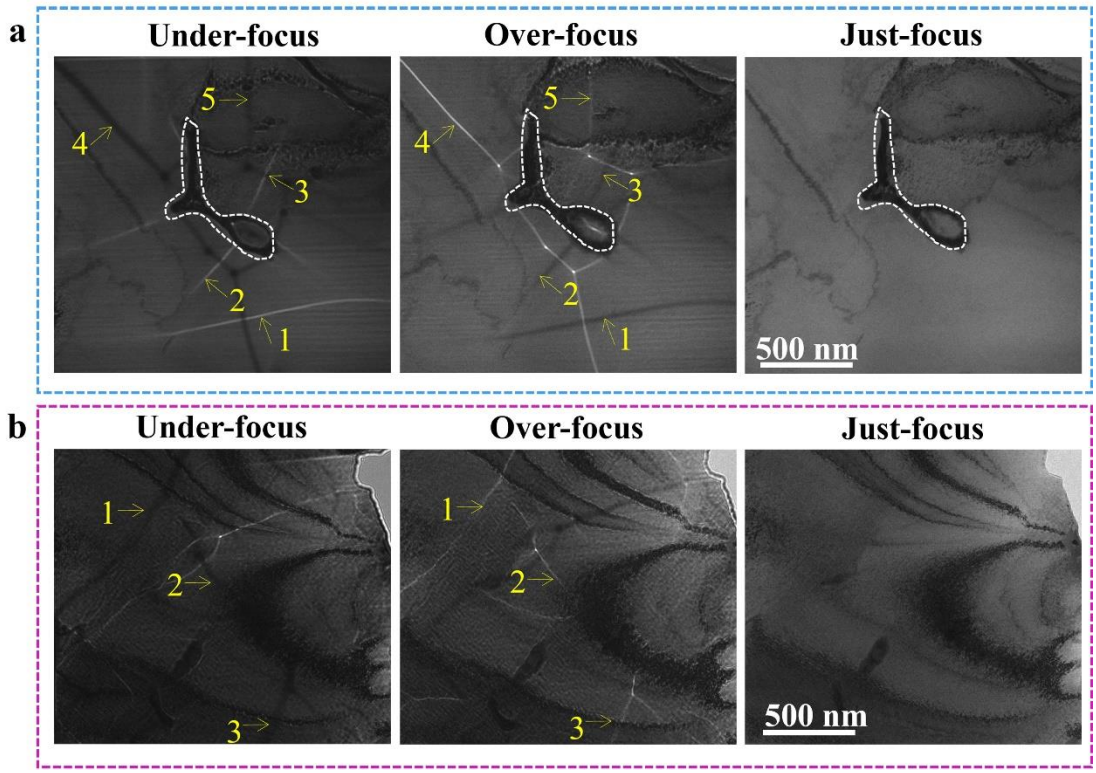

Figure S8. Lorentz TEM (LTEM) images taken from **a** as-spun and **b** 800 ℃ - 120 min HEA fibers. The magnetic domain walls are indicated by yellow arrows.

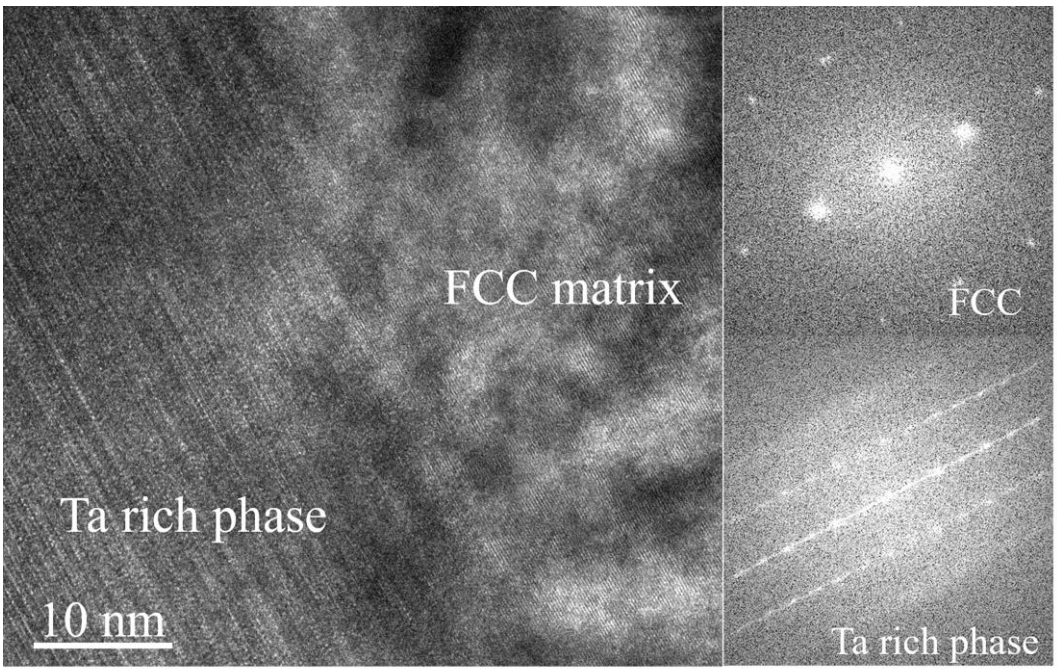

Figure S9. HRTEM image and corresponding FFT patterns of the Ta-rich phase in as-spun HEA fibers.

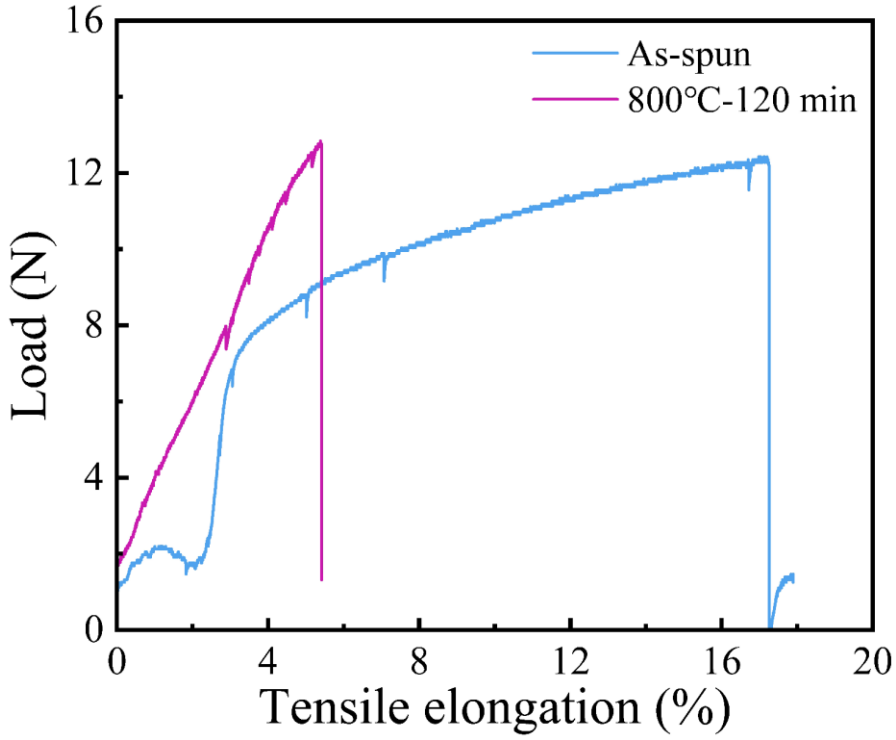

Figure S10. Tensile strain-load curves of *in-situ* tensile tests of as-spun and 800 ℃-120 min annealed HEA fibers. Source data for Figure S10 are provided as a Source data file.

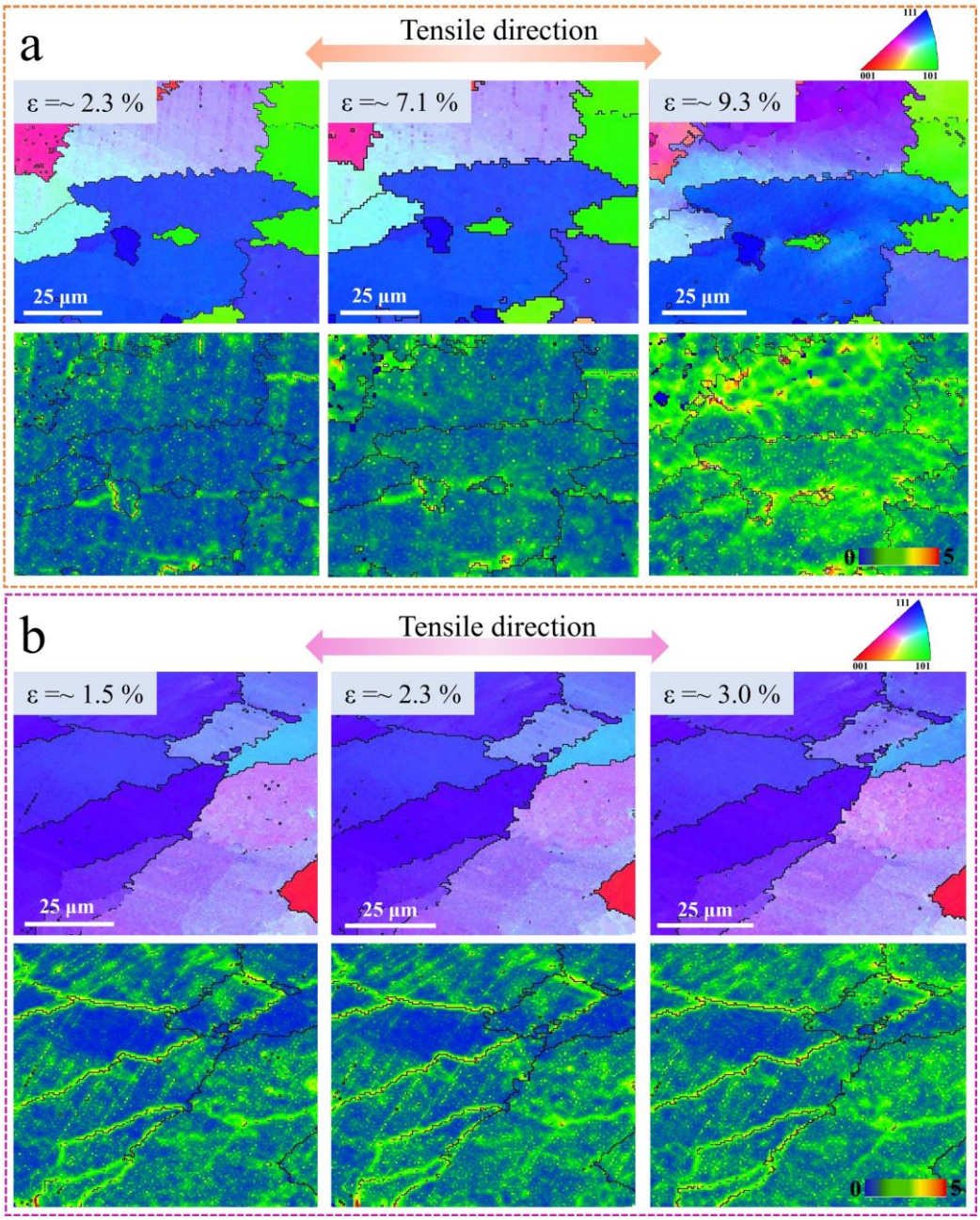

Figure S11. *In-situ* EBSD and KAM observation of **a** as-spun and **b** 800 ℃-120 min annealed HEA fibers at different tensile strain. The areas with high KAM values are inside the grains for the as-spun fibers. The areas with high KAM values are located at grain boundaries for the 800 ℃-120 min annealed fibers.

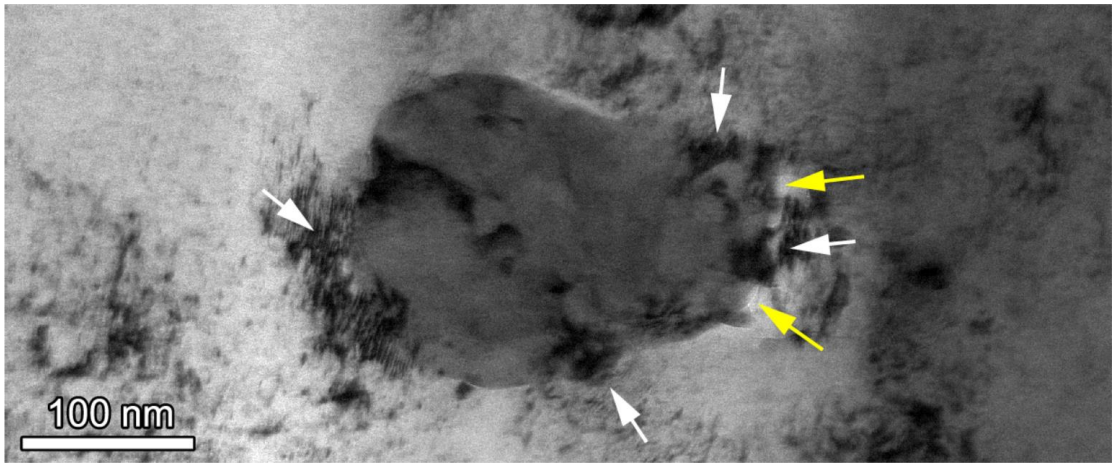

Figure S12. TEM observation of a $(Ta_2(Co/Fe/Ni)_3Si$ particle in the as-spun HEA fiber after deformation, where dislocation pile-ups are indicated by white arrows, micro-voids are indicated by yellow arrows.

Table S1. Summary table of coercivity and tensile-strain of typical soft magnetic fibers.

Compositions	Coercivity (Oe)	Tensile strain (%)	Ref.
$Fe_{77}Si_8B_{15}$	53.1	4	[1]
$Fe_{77}Si_8B_{15}$	35.0	4	[1]
$Fe_{77}Si_8B_{15}$	36.5	4	[1]
$Fe_{77}Si_8B_{15}$	25.4	4	[1]
$Fe_{77}Si_8B_{15}$	10.0	4	[1]
$Fe_{77}Si_8B_{15}$	7.5	4	[1]
$Fe_{77}Si_8B_{15}$	4.4	4	[1]
$Fe_{67}Co_{18}B_{14}Si_1$	0.05	3.8	[2]
$Fe_{80}B_{20}$	0.08	3.4	[1, 2]
$Fe_{59}Ni_{15}B_{13}Si_{11}C_2$	1.2	2.4	[1, 2]
$Fe_{47}Ni_{27}Si_{11}B_{13}C_2$	0.76	2.5	[1, 2]
$Fe_{90}Si_5B_5$	9.3	0.62	[3]
$Fe_{78}B_{13}Si_9$	0.03	4	[1, 4]
$Fe_{78}B_{13}Si_9$	0.09	2	[1, 4]
$Fe_{80}P_{12}C_8$	0.1	5	[5, 6]
$Fe_{80}P_{11}C_8B$	0.05	4	[5, 6]
$Fe_{80}P_{10}C_8B_2$	0.04	3	[5, 6]
$Fe_{80}P_9C_8B_3$	0.05	2	[5, 6]
$Fe_{80}P_8C_8B_4$	0.04	0.5	[5, 6]
$Fe_{76}Si_{13}B_8Nb_2Cu_1$	0.25	2	[7]
$Fe_{68.5}Co_5Ta_3Cu_1Si_{16.5}B_6$	0.66	1.5	[8]
$Fe_{90}Si_{10}$	56.9	6.75	[9]
$Fe_{50}Ni_{50}$	0.12	3	[10]
$Fe_{20}Ni_{80}$	0.02	4	[10]
$Fe_{35}Ni_{65}$	0.08	3	[10]
$Co_{80}Si_{10}B_{10}$	12.9	0	[1]
$Co_{68.15}Fe_{4.35}Si_{12.5}B_{15}$	2.6	0	[1]
$Co_{68.15}Fe_{4.35}Si_{12.5}B_{15}$	2.5	0	[1]
$Co_{68.15}Fe_{4.35}Si_{12.5}B_{15}$	4.9	0	[1]
$Co_{80}Si_{10}B_{10}$	10.3	0	[1]
$Fe_{29}Co_{71}$	37.5	5	[11]
$Fe_{29}Co_{71}$	18.3	8.9	[11]
$Fe_5Co_{71}Si_{10}B_{11}Cr_3$	0.06	1.7	[12]
$Fe_{3.8}Co_{67}Ni_{1.5}B_{11.5}Si_{14.5}Mo_{1.7}$	0.26	1.6	[12]
$Co_{69}Fe_{5.5}Ni_1Si_{14.5}B_{10}$	0.03	1.8	[13]
$Co_{69}Fe_{5.5}Ni_1Si_{13.5}P_1B_{10}$	0.02	1.5	[13]
Carbon fiber@Fe	119.7	1.1	[14]
Carbon fiber@Ni	80.8	1	[14]
Carbon fiber@FeCo	38.9	0.8	[14]
Carbon fiber@FeNi	28.9	0.7	[14]
$Fe_{34}Co_{29}Ni_{29}Al_3Ta_3Si_2$	8.1	23	This work

Table S2. Curie temperatures and lattice parameters of as-spun and 800 ℃-120 min annealed HEA fibers.

	Curie temperature (K)	Lattice parameters (Å)
As-spun	770	$a=b=c=3.582$
800 ℃-120 min	690	$a=b=c=3.582$

References

[1] H. Chiriac, *et al.* Amorphous glass-covered magnetic wires: preparation, properties, applications, *Prog. Mater. Sci.* **40**, 333-407 (1996).

[2] Y. Kefu, *et al.* Research progress and application prospect of Fe-based soft magnetic amorphous/nanocrystalline alloys, *Acta. Phys. Sin-Ch. Ed* **67**, 016101 (2018).

[3] Y. Han, *et al.* Syntheses and fundamental properties of Fe-rich metastable phase alloys with saturation magnetization exceeding 1.9 T, *Mater. Res.* **100**, 367-370 (2015).

[4] J. Zhang, *et al.* Thin and flexible Fe-Si-B/Ni-Cu-P metallic glass multilayer composites for efficient electromagnetic interference shielding, *ACS Appl. Mater. Inter.* **9**, 42192-42199 (2017).

[5] M. Shi, *et al.* Effects of metalloid B addition on the glass formation, magnetic and mechanical properties of FePCB bulk metallic glasses, *J. Mater. Sci. Technol.* **31**, 493-497 (2015).

[6] Z. Shi, *et al.* Controllable brittleness in soft-magnetic Fe-P-C-B metallic glasses through composition design, *Mater. Sci. Eng. A* **766**, 138385 (2019).

[7] Z. Ma, *et al.* Ultrathin, flexible, and high-strength Ni/Cu/metallic glass/Cu/Ni composite with alternate magneto-electric structures for electromagnetic shielding, *J. Mater. Sci. Technol.* **81**, 43-50 (2021).

[8] N.M. Bruno, *et al.* The effect of stress-annealing on the mechanical and magnetic properties of several Fe-based metal-amorphous nano-composite soft magnetic alloys, *J. Non-Cryst. Solids* **600**, 122037 (2023).

[9] M. Yazdanmehr, *et al.* Using GA-ANN algorithm to optimize soft magnetic properties of nanocrystalline mechanically alloyed Fe-Si powders, *Com. Mater. Sci.* **44**, 1218-1221 (2009).

[10]https://openstd.samr.gov.cn/bzgk/gb/newGbInfo?hcno=6660CA9CC366499101A7B02CCCE7A72A.

[11] T. Yamazaki, *et al.* Microstructure-enhanced inverse magnetostrictive effect in Fe-Co alloy wires, *Adv. Eng. Mater.* **22**, 2000026 (2020).

[12] A. Zhukov, *et al.* Magnetostriction of Co-Fe-Based amorphous soft magnetic microwires, *J. Electron. Mater.* **45**, 226-234 (2016).

[13] S. Shuai, *et al.* Stress-induced giant magneto-impedance effect of amorphous CoFeNiSiPB ribbon with magnetic field annealing, *J. Magn. Magn. Mater.* **551**, 169131 (2022).

[14] Y. Zhang, *et al.* Enhanced magnetoimpedance effect of carbon fiber/Fe-based alloy coaxial composite by tensile stress, *Carbon* **93**, 451-457 (2015).